International Journal of High Speed Electronics and Systems
Vol. 19, No. 1 (2009) 33 – 53

World Scientific
www.worldscientific.com

EMISSION AND INTENSITY MODULATION OF TERAHERTZ ELECTROMAGNETIC RADIATION UTILIZING 2-DIMENSIONAL PLASMONS IN DUAL-GRATING-GATE HEMT'S

TAIICHI OTSUJI

Research Institute of Electrical Communication, Tohoku University, 2-1-1 Katahira, Sendai, Miyagi 980-8577, Japan
otsuji@riec.tohoku.ac.jp

TAKUYA NISHIMURA

Research Institute of Electrical Communication, Tohoku University, 2-1-1 Katahira, Sendai, Miyagi 980-8577, Japan

YUKI TSUDA

Research Institute of Electrical Communication, Tohoku University, 2-1-1 Katahira, Sendai, Miyagi 980-8577, Japan

YAHYA MOUBARAK MEZIANI

Research Institute of Electrical Communication, Tohoku University, 2-1-1 Katahira, Sendai, Miyagi 980-8577, Japan

TETSUYA SUEMITSU

Research Institute of Electrical Communication, Tohoku University, 2-1-1 Katahira, Sendai, Miyagi 980-8577, Japan

EIICHI SANO

Research Center for Integrated Quantum Electronics, Hokkaido University, N13W8, Sapporo, Hokkaido 060-8628, Japan

Two dimensional plasmons in submicron transistors have attracted much attention due to their nature of promoting emission/detection of electromagnetic radiation in the terahertz range. We have recently proposed and fabricated a highly efficient, broadband plasmon-resonant terahertz emitter. The device incorporates doubly interdigitated grating gates and a vertical cavity into a high electron mobility transistor. The device operates in various modes: (1) DC-current-driven self oscillation, (2) CW-laser excited terahertz emission, (3) two-photon injection-locked difference-frequency terahertz emission, and (4) impulsive laser excited terahertz emission. Furthermore, the device can operate in completely different functionalities including ultrahigh-speed intensity modulation for terahertz carrier waves. This paper reviews recent advances on plasma wave devices.

Keywords: Terahertz; plasmon; resonance; emitter; instability; injection locking; intensity modulator

1. Introduction

"Terahertz" is an unexplored frequency band in the sense that there is no commercially available microelectronic device that can generate, detect, or manipulate electromagnetic waves over the entire terahertz frequency band[1]. In the last decade, then therefore, development of compact, tunable and coherent sources operating at terahertz frequencies has been one of the hottest issues of the modern terahertz (THz) electronics[1]. Two dimensional (2D) plasmons in submicron transistors have attracted much attention due to their nature of promoting emission of electro-magnetic radiation in the terahertz range[2-5]. We have recently proposed and fabricated a highly efficient, broadband plasmon-resonant terahertz emitter/photomixer device[6-11]. The device incorporates doubly interdigitated grating gates and a vertical cavity into a semiconductor heterojunction high electron mobility transistor (HEMT) so that structure-dependent highly dispersive plasmonic systems can be configured in submicron-to-nanometric scaled artificial dimensions to perform emission, detection, and moreover higher functional signal processing like intensity modulation as well as frequency multiplication in an exploring terahertz frequency region. Test samples are fabricated using InGaP/InGaAs/GaAs material systems, succeeding in the first observation of stimulated emission of terahertz radiation at room temperature. This article reviews recent advances in novel plasmonic nanotransistors for emission and intensity modulation of terahertz electromagnetic waves. and presents a new result on photomixed injection locked oscillation.

2. Plasmon-Resonant Terahertz Emitter

2.1. *Device structure and operation principle*

Figure 1 illustrates the cross section of the plasmon-resonant emitter. The device structure is based on a high electron mobility transistor (HEMT) and incorporates (i) doubly interdigitated grating gates (G1 and G2) that periodically localize the 2D plasmon in stripes on the order of 100 nm with a micron-to-submicron interval and (ii) a vertical cavity structure in between the top grating plane and a terahertz mirror at the backside. The structure (i) works as a terahertz antenna[12] and (ii) works as an amplifier. The terahertz mirror is to be a transparent metal like indium titanium oxide (ITO) when the device works in an optical excitation mode so as to excite the plasmons by optical two-photon irradiation from outside the back surface[6].

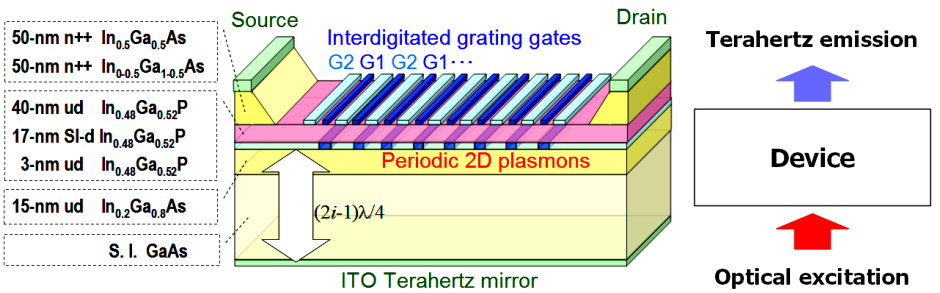

Fig. 1. Device cross section for typical GaAs-based heterostructure material systems. k: the wave vectors of irradiated photons, E_x: the electric field (linear polarization), k_{THz}: the wave vector of electromagnetic radiation.

Suppose that the grating gates have geometry with 300-nm G1 fingers and 100-nm G2 fingers to be aligned alternately with a space of 100 nm and that an appropriately high 2D electronic charge (~10^{12}cm^{-2}) is induced in the plasmon cavities under G1 while the regions under G2 are weakly charged (10^{10}~10^{11}cm^{-2}). Figure 2 depicts a numerically simulated typical 2D electron density/velocity distributions based on a self-consistent drift-diffusion Poisson equations. A standard DC drain-to-source bias V_{DS} of 50 mV/(grating period), and the gate biases V_{G1} and V_{G2} of V_{th} + 2.2 V and V_{th} + 0.2 V are assumed where V_{th} is the threshold voltage. As is seen in Fig. 2, a strong electric field (1~10 kV/cm) arises at the plasmon cavity boundaries[11]. When the DC drain-to-source bias V_{DS} is applied, 2D electrons are accelerated to produce a constant drain-to-source current I_{DS}. Due to such a distributed plasmonic cavity systems with periodic 2D electron-density modulation, the DC current flow may excite the plasma waves in each plasmon cavity. As shown in Fig. 3, asymmetric cavity boundaries make plasma-wave reflections as well as abrupt change in the density and the drift velocity of electrons, which may cause the current-driven plasmon instability[3, 13, 14, 15] leading to excitation of coherent resonant plasmons. Thermally excited hot electrons also may excite incoherent plasmons[16-20]. The grating gates act also as terahertz antenna that converts non-radiative longitudinal plasmon modes to radiative transverse electromagnetic modes[6].

When the device is photoexcited by laser irradiation, photoelectrons are predominantly generated in the weakly-charged regions with many unoccupied electronic states under G2 and then are injected to the plasmon cavities under G1. Thanks to a specific drain-to-source bias promoting a uniform slope along the source-to-drain direction on the energy band in the regions under G2, photoelectrons under G2 are unidirectionally injected to one side of the adjacent plasmon cavity. This may also excite the plasmons under an asymmetric cavity boundary[3, 4, 21]. It is noted that the laser irradiation may excite the plasmon not only in the regions under G1 but also in the regions under G2 if the cavity size and carrier density of the regions under G2 also satisfies the resonant conditions.

Once the terahertz electromagnetic waves are produced from the seed of plasma waves, downward-propagating electromagnetic waves are reflected at the mirror back to

the plasmon region so that the reflected waves can directly excite the plasmon again according to the Drude optical conductivity and intersubband transition process[6]. When the plasmon resonant frequency satisfies the standing-wave condition of the vertical cavity, the terahertz electromagnetic radiation will reinforce the plasmon resonance in a recursive manner. Therefore, the vertical cavity may work as an amplifier if the gain exceeds the cavity loss. The quality factor of the vertical cavity is relatively low as is

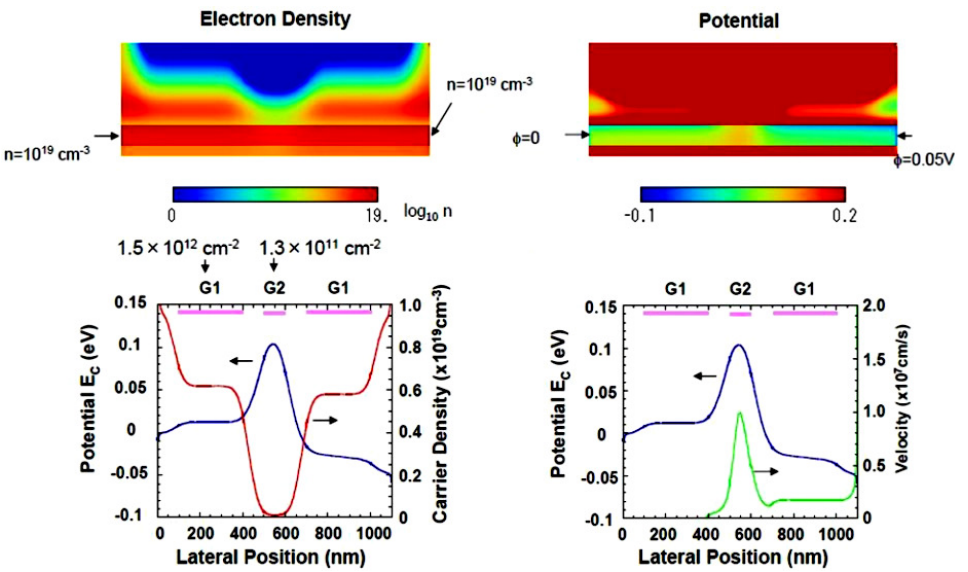

Fig. 2. Electron density/velocity distributions in a unit of the 2D plasmon grating cavities. V_{DS} = 50 mV/(grating period), $V_{G1} = V_{th} + 2.2$ V, $V_{G2} = V_{th} + 0.2$ V. (after Ref. 11.)

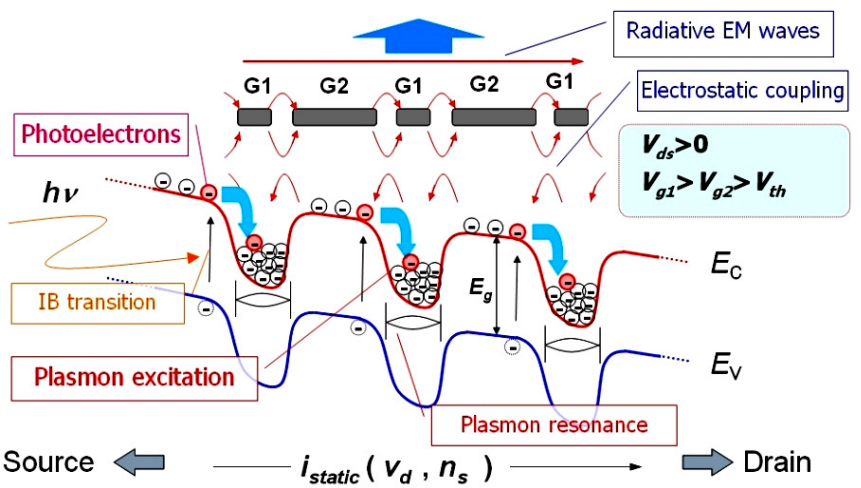

Fig. 3. Schematic band diagram and operation mechanism. (after Ref. 11.)

simulated in Refs. 6, 22 since the 2D plasmon grating plane of one side of the vertical cavity boundary must have a certain transmittance for emission of radiation. Thus, the cavity serves a broadband character.

2.2. *Characteristic parameters and design scheme*

Field emission properties of the dual-grating-gate plasmon-resonant emitters are characterized by the structure dependent key parameters shown in Fig. 4[6, 22]. The primary parameter that initiates the plasmon resonance is ω_{p2} which is the plasma frequency, i.e. plasmon characteristic frequency, of the periodically confined *gated* plasmon cavities. Each cavity is connected by the connecting portion whose carrier density must be controlled to be far apart from that in the plasmon cavity to make a good plasmon confinement. Thus, this connecting portion has its characteristic frequency ω_{p3}. The grating gate has also its own plasma frequency ω_{p1}. Note that ω_{p2} and ω_{p3} for the *gated* plasmon cavities and connecting portions obey the linear dispersion law while ω_{p1} for the *ungated* gate gratings is proportional to the square-root of wave vector[3, 6, 13]. All the three parameters are mainly determined by their cavity length: W, the distance between layers: d, and carrier density, and perturbed by their periodicity: a, or the filling parameter: $f = W/a$ [13]. The final parameter, denoted by ω_L, corresponds to the vertical cavity resonance.

According to the operating frequency band, the grating geometry (single plasmon cavity length and periodicity) is designed to be fixed and ω_{p1} and ω_{p3} as well as ω_L are optimally designed. For an actual device operation, ω_{p2} is a given parameter, which is first tuned by the gate bias at a specific value to obtain a desired resonance frequency. As a fundamental design criterion to obtain high quantum efficiency, ω_{p1} and ω_L values are to be matched to ω_{p2} value while ω_{p3} is far depart from them. Once the device dimensions and material systems are designed, ω_{p1} and ω_L become fixed parameters. ω_{p3} for the connecting portion, on the other hand, is controllable (by V_{g2}) so that one can set it at far higher or lower than ω_{p2} by making the connecting portion to be metallic or dielectric. When the grating gate is made with metals like standard HEMT's, ω_{p1} becomes higher by orders of magnitude than ω_{p2}, resulting in degrading the emission power/efficiency[6, 21]. To prevent it, a semiconducting material, in particular, 2DEG grating gate made from the upper deck of a double-decked HEMT is superior[11, 23, 24], which is demonstrated in Sec. 5.

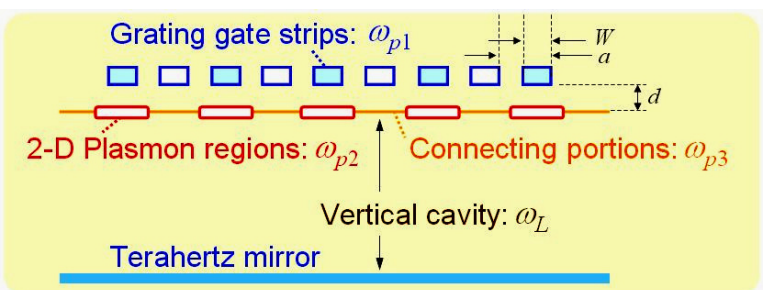

Fig. 4. Characteristic frequencies. (after Ref. 6.)

The plasma wave behavior of the 2D electron systems (2DES) is described by the extended Dyakonov-Shur model[3, 6]. Under the gradual channel approximation, the local electron density n and velocity v of the plasma fluid are formulated by the hydrodynamic equations:

$$m_e\left(\frac{\partial \boldsymbol{v}}{\partial t}+(\boldsymbol{v}\cdot\nabla)\boldsymbol{v}\right)=-e\nabla U-m_e\frac{\boldsymbol{v}}{\tau}\ , \tag{1}$$

$$\frac{\partial n}{\partial t}+\nabla(n\boldsymbol{v})=\frac{\partial U}{\partial t}+\nabla(U\boldsymbol{v})=0\ , \tag{2}$$

where m_e the electron effective mass, e the electronic charge, U the gate-to-channel potential, τ the plasmon relaxation time. Their time-evolved response to the terahertz excitation is numerically analyzed using the finite differential time-domain (FDTD) method. The plasma waves themselves are the coherent electronic polarization so that they should produce local displacement AC current. Thus, it is input to the Maxwell's FDTD simulator as a current source to analyze the electromagnetic field dynamics.

Figure 5 shows typical instantaneous cross-sectional distribution of the electric-field intensity along the x (source to drain) direction under a constant sinusoidal plasmon excitation at (a) a tuned frequency of 3.4 THz and (b) a detuned frequency of 5.1 THz[6]. The device model is based on the HEMT shown in Fig. 1 accommodating nine periods of the dual grating gates. The gate finger lengths, L_{G1} and L_{G2}, of 200 and 900 nm with 100-nm spacing are assumed. The characteristic frequencies ω_{p1} and ω_L are set at 3.4 THz. The primary parameter ω_{p2} are set at the excitation frequency (3.4 THz for (a) and 5.1 THz for (b)). All the plasmon cavities are excited in phase. One can see in Fig. 5 (a) an in phase oscillation between outside air (upper portion) and inside the cavity since the vertical cavity length is set at the quarter wavelength of the fundamental mode. The white colored area shows very high intensity of over the range. Under a detuned condition of 5.1-THz excitation, on the other hand, antiphase oscillation is seen as is expected. The radiation power is almost remained at the level of that for the tuned condition. For both cases, the periodic longitudinal polarization in the plasmon grating plane is satisfactorily

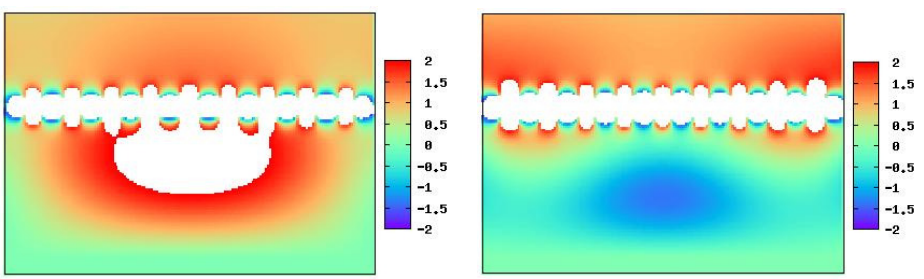

(a) (b)

Fig. 5. Simulated instantaneous electric field (E_x) distributions under a constant sinusoidal plasmon excitation (a) at 3.4 THz and (b) 5.1 THz. Intensity scaled on the indicator is in arbitrary unit. (after Ref. 6.)

converted to the transverse monotonic electric field in the outside the device (upper portion in Fig. 5). The results clearly show the standing wave oscillation inside the cavity and forward propagating quasi-transverse electromagnetic (TEM) waves outside in air.

In order to examine how the double gate grating and vertical cavity structures contribute to the field emission properties, artificial structures without double gate grating and/or terahertz mirror are prepared for, and compared their impulse responses to that of original structure by using Maxwell's FDTD simulator[6]. All the characteristic parameters were fixed at the nominal values (ω_{p1}= ω_{p2}= ω_L=3.4 THz). Each plasmon cavity was excited with an impulsive current source simultaneously. Simulated temporal responses of the electric field (*x* component) at the central two points (4 μm beyond the gate surface and 4 μm beneath the plasmon surface) were Fourier transformed to obtain entire frequency spectra.

Figure 6 plots the results[6]. For the structures without gate gratings, neither *gated* plasmon modes nor the Smith-Purcell effect is produced resulting in no obvious field enhancement over the frequency range; a small dip below 1THz is an unphysical error caused in numerical process. The vertical cavity makes a resonance property and weakly enhances the radiation in narrow bands around the fundamental and second harmonic frequencies.

Incorporating the double gate grating, on the contrary, produces extraordinary electromagnetic transmission; the electric field intensity drastically enhances over a broadband range. As a result, mode-conversion gain, from non-radiative plasmon mode to radiative mode, of up to 14dB (a factor of 5) was successfully obtained in a wide frequency range from 600 GHz to 4 THz corresponding to the fundamental plasmon

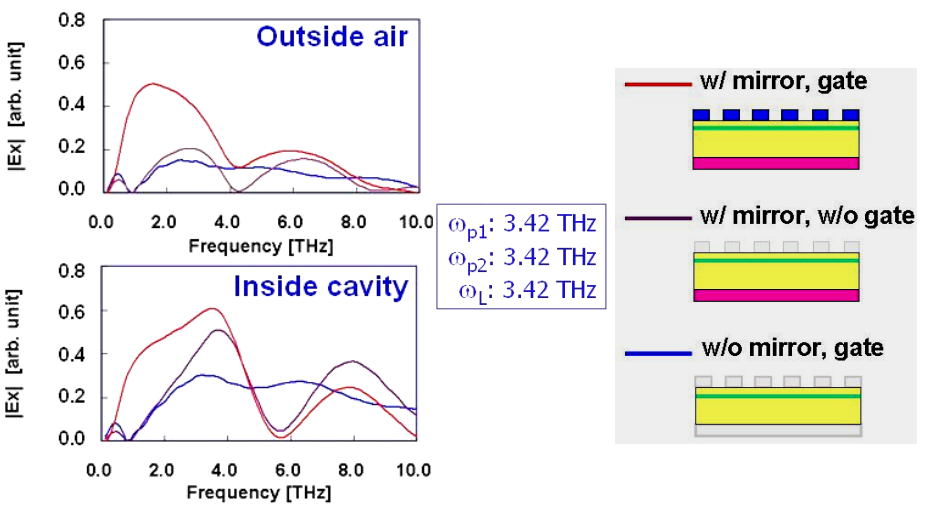

Fig. 6. Simulated frequency responses for three different device structures to impulsive excitation at all the plasmon cavities. Electric fields (*x* component) at two points (inside the cavity and outside air) are calculated by using a Maxwell's FDTD simulator and their temporal profiles were Fourier transformed. (after Ref. 6.)

resonance. One can see the fundamental peak stays at around 1.8 THz outside the air, which is fairly lower than the original characteristic frequency of ω_{p2}. One possibility for this cause would be the excitation of vertically coupled surface plasmon polaritons as is seen in the interfaces of metallic gratings[25]. It is noted that the wavelength under consideration is by two orders of magnitude larger than the feature size of the grating, which is thought to be a consequence of excitation of complex plasmon modes produced in the grating-bicoupled unique structure.

2.3. *Device fabrication*

The device was fabricated with InGaP/InGaAs/GaAs material systems in two structures: a standard single-heterostructure HEMT with metallic grating gates[7-11] and a double-decked (DD) HEMT with semiconducting two-dimensional electron gas (2DEG) grating gates[11, 23, 24]. The SEM (scanning electron microscopy) images for a typical metal-grating sample are shown in Fig.7(a). The 2D plasmon layer is formed with a quantum well at the heterointerface between a 15-nm thick undoped InGaAs channel layer and a 60-nm thick, Si-δ doped InGaP carrier-supplying layer. The grating gate was formed with 65-nm thick Ti/Au/Ti by a standard lift-off process. To cover operating frequencies from 1 to 10 THz, the grating geometry was designed with 350-nm G1 fingers and 100-nm G2 fingers to be aligned alternately with a space of 70 nm. The gate width is 75 μm for both G1 and G2. For comparison, another sample having a larger fraction in G1/G2 fingers (1800 nm/100 nm) was also fabricated. The number of gate fingers G1/G2 is 61/60 (38/37) for the sample having 300-nm (1800-nm) G1 fingers.

The device cross sectional view and its SEM image of a semiconducting grating-gate device are shown in Fig. 7(b)[23]. In this work, in order to produce the periodically-localized 2DEG, the double-decked HEMT structure is employed. The upper deck channel serves as the grating-gate antenna and is then periodically etched. Therefore more intensity in the emitted THz wave is expected. The HEMT structure consists of the InGaP/InGaAs/GaAs heterostructure with a selective doping in the InGaP layer. For the source/drain ohmic contacts, AuGe/Ni was lifted off and annealed after the upper-deck HEMT was selectively etched. The intrinsic device area is 30×75 μm^2, where the grating pattern is replicated on the upper-deck HEMT layer. The grating consists of 80-nm lines and 350-nm lines aligned alternately with a spacing of 100 nm. The number of fingers is 60 (61) for the 80-nm (350-nm) grating.

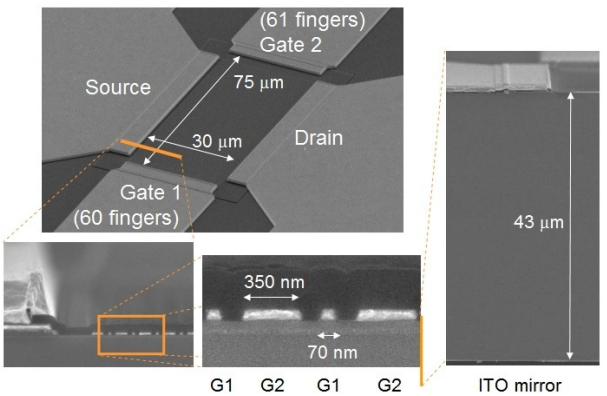

(a)

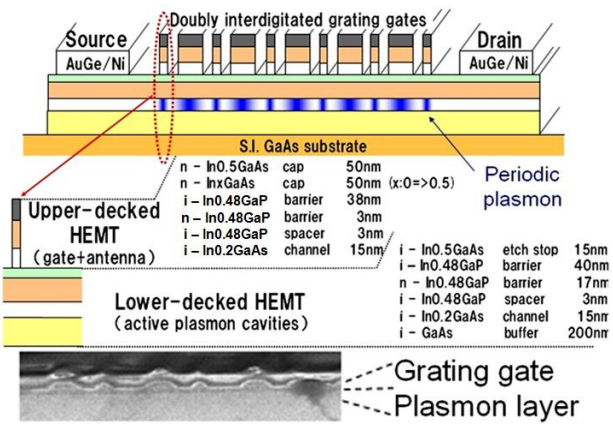

(b)

Fig. 7. SEM images of a fabricated metal grating-gate (a) and semiconducting grating-gate (b) plasmon-resonant emitter. (After Ref. 24.)

2.4. *Experimental Results and Discussions*

2.4.1. *DC-current-driven self oscillation*

Fourier-transformed far-infrared spectroscopic (FTIR) measurements were carried out for those samples[10, 11, 23, 24]. The samples were placed in the source position of the vacuum cavity of the FTIR. The radiation intensity was measured by Si bolometer having a responsivity of 2.84×10^{5} V/W and a noise-equivalent power (NEP) 1.16×10^{-13} W/Hz$^{1/2}$. The experimental procedure was following – first we measured the background spectra – the spectra without any current flowing through the sample. This spectra contained information of the 300K blackbody emission modified by the spectral functions of all the elements inside the spectrometer. Then we measured the spectra with current flowing through the sample, and then, normalized them to the background data.

FTIR measured emission spectra for metal-grating gate samples having L_{G1}/L_{G2} = 70 nm/1850 nm and L_{G1}/L_{G2} = 70 nm/350 nm are shown in Fig. 8 (a) and (b), respectively[10, 11, 24]. One can see relatively broad spectra starting from about 0.5 THz with maxima around 2.5 THz for the first sample (S1) and around 3.0 THz for the second one (S2); the grating geometry reflects the spectral profile. For both samples the emission dies off abruptly around 6.5 THz, which is thought to be due to the Reststrahlen band of optical phonon modes of the GaAs-based materials[10].

The emission intensity versus V_{DS} is shown in Fig. 8(c). One can see that the emission intensity has a threshold property against V_{DS} and has a super-linear (nearly quadratic) dependence on V_{DS}. It is considered that the former property reflects on the coherent plasmons excited by the plasmon instability[3, 14, 15], while the latter property is attributed to the emission caused by the thermally excited incoherent plasmons due to injection of drifting hot electrons into the plasmon cavities[10, 24, 26, 27].

FTIR measured spectra for semiconducting-grating gate samples having L_{G1}/L_{G2} = 150 nm/1850 nm are shown in Fig. 9[11, 24]. It is, an intense emission power of the order of 1 μW for the DD-HEMT's at 300K (one order of magnitude higher than that for MGG-HEMT's). Dyakonov-Shur plasmon instability[3] and/or the Ryzhii-Satou-Shur transit-time instability[14, 15] may take place at the cavity boundaries where the electron drift velocity (thus, 2DEG density) modulation predominantly occurs. Analytical calculation suggests that the instabilities are critically promoted near the drain side with low 2DEG densities when V_{DS} exceeds the pinch off, resulting in the above-mentioned threshold property and enhancement of the emission at low frequency region around 2 THz . Since usually these coherent plasmons excitations are believed to have sharp spectral features, the observed spectral peaks may be attributed to these instability-driven emission.

The emission spectrum of thermally excited plasmons of the metallic grating-gate structure was calculated based on a first-principles electromagnetic approach elaborated upon in Refs. 26 and 27 where only a single metal grating in the structure is assumed as shown with solid lines in Fig. 8(a)[10]. In the calculated single-period structure spectrum, the fundamental plasmon resonance appears at around 3 THz and the second one at about 4.5 THz. This may explain a pronounced bump around 5 THz in the high-frequency shoulder in the short period structure experimental spectrum. The plasmon spectra in the actual double-grating structure in question, of course, must be more complex compared to that in a single-grating structure modeled numerically. In principle two different sorts of plasmon cavities can be formed under the metal fingers of different width in the double-grating structure.

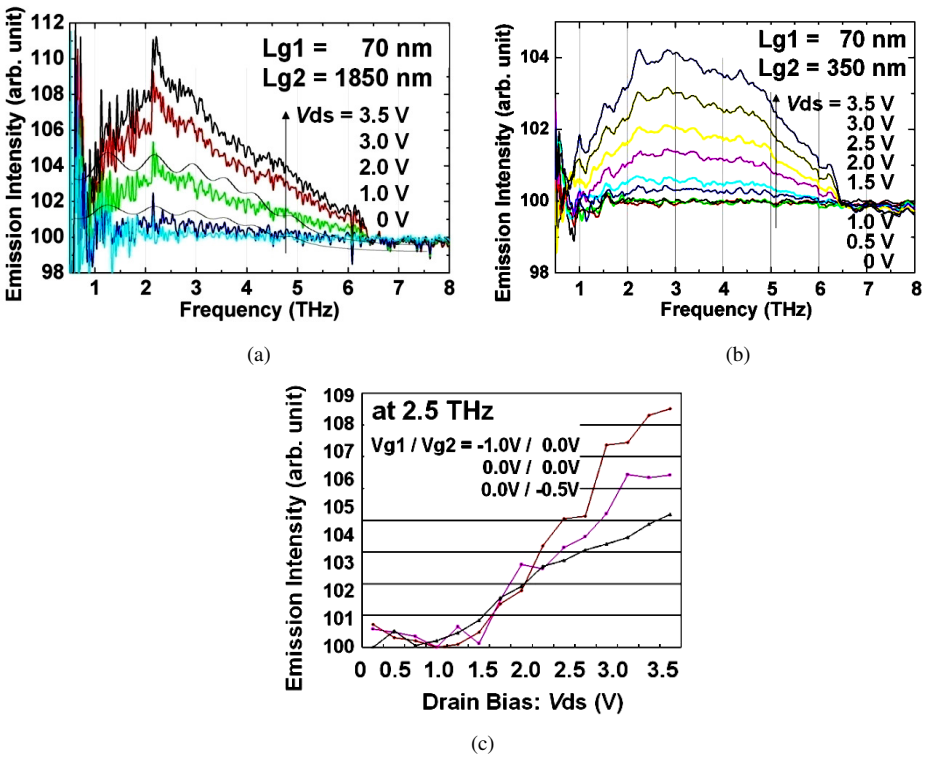

Fig. 8. FTIR measured emission spectra for metal-grating gate samples at room temperature. (a) L_{G1}/L_{G2} = 70 nm/1850 nm, (b) L_{G1}/L_{G2} = 70 nm/350 nm. The grating geometry reflects the emission spectra. (c) emission intensity at 2.5 THz vs. *V*ds for the sample with L_{G1}/L_{G2} = 70 nm/1850 nm, showing threshold behavior and super-linear (near quadratic) dependence on *V*ds. Two solid lines in (a) are calculated results for emissions from thermally excited plasmons at electronic temperatures of 310K and 320K. (after Ref. 24.)

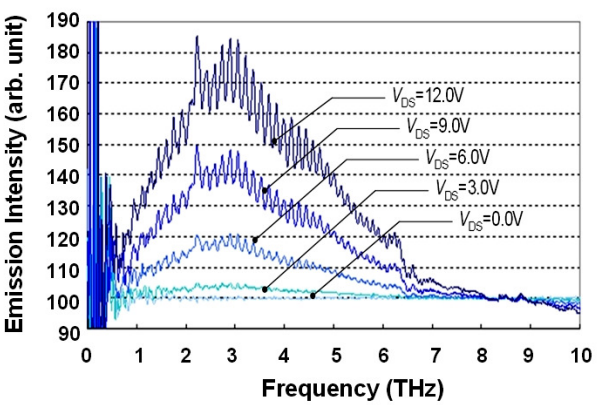

Fig. 9. FTIR measured emission spectra for a semiconducting grating-gate sample with L_{G1}/L_{G2} = 150 nm/1850 nm at room temperature. (after Ref. 24.)

2.4.2. *CW-pumped optically excited stimulated terahertz emission*

Next, the device was irradiated from the backside with a lineally-polarized 1550-nm band CW laser beam to measure its photoresponse at room temperature[8, 9]. A 1550-nm band tunable laser source with an average power of 2 mW was used. The polarization is set to be in parallel to the channel direction. Actually, the photon energy of the irradiated laser is much lower than all the band gap energies of this material system. However, the electrons are weakly photoexcited at the InGaAs/GaAs heterointerface via multi-step processes due to the existence of deep trap centers[27]. The photoelectrons are injected to the channel immediately due to the strong gate-to-channel electric field.

When the plasma wave resonance is excited, the DC drain-source potential is modulated because of the non-linear properties of the plasma fluid[4]. Therefore, the resonant intensity was measured by monitoring the DC modulation component ΔV_{DS} of the drain potential, which is called hereafter the photoresponse. The variation in ΔV_{DS} under irradiation was precisely lock-in amplified and detected at a chopping frequency of 1.29 KHz. At the same time, the terahertz radiation was detected using a 4.2-K cooled Silicon bolometer with a filter pass band from 0.6 to 3.5 THz.

Typical results for the V_{G1} and V_{G2} dependence of the photoresponses of a metal grating-gate sample (L_{G1}/L_{G2} = 300 nm/100 nm) for different V_{DS} conditions are shown in Fig. 10 [8, 9]. The device exhibited a marked photoresponse with relatively sharp peaks on its V_{G2} dependence and with broad peaks on its V_{G1} dependence. For V_{G2} dependence, when V_{DS} = 1.0 V, the photoresponse exhibited a clear single peak at V_{G2} = -1.9 V. According to the Dyakonov-Shur model[4] this photoresponse peak at the lowest gate bias is interpreted as the fundamental plasmon resonance. With increasing in V_{DS} up to 3.0 V, the single peak becomes steeper and shifts up to higher V_{G2} point at around 0 V while the secondary peak grows up at lower V_{G2} point at -3.0 V, corresponding to the third-harmonic plasmon resonance. Similarly, for V_{G1} dependence, when V_{DS} increases from 1.0 to 3.0 V, weak double dips on the background slope at V_{DS} = 1.0 V grows up to clear double peaks at V_{G1} = -0.8 V and -2.8 V.

The results are completely different from that for standard HEMT devices having a single-gate finger fabricated on the same wafer showing monotonic dependence on the gate bias (plotted with a broken line in Fig. 10(a). Theoretical investigations in Refs. 3 and 13 suggest that the plasmon instability is promoted when electrons have a very high drift velocity of around 4×10^7 cm/s (equivalent plasma-wave Mach number of around 0.5). Carrier dynamics under weakly photoexcited conditions in our device are simulated based on an extended drift-diffusion model[29]. The result indicates that the injection of photoelectrons from a weakly charged 2DEG to the adjacent deeply charged 2DEG (plasmon cavity) is performed in a quasi-ballistic manner so that the above-mentioned instability condition is obtainable.

Focused on a simplest case at V_{DS} = 1.0 V, terahertz emission from the device was measured by using a 4-K cooled Si bolometer. At the same time, the device photoresponse was also measured. The measured results are plotted onto the V_{G1}-V_{G2} space as shown in Fig. 11(a) and (b)[9]. The photoresponse in Fig. 11(a) exhibits local

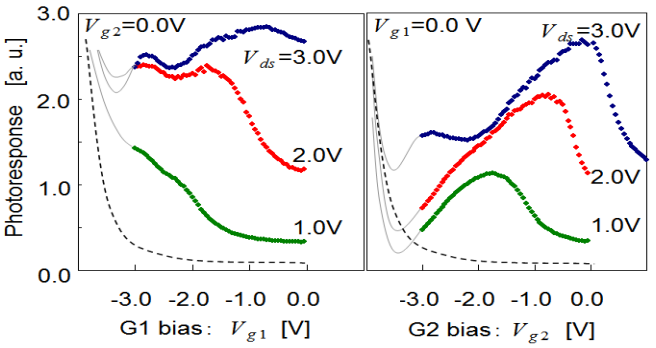

Fig. 10. Measured photoresponse to a single CW laser irradiation for a metal grating-gate sample having a grating gates geometry of L_{G1}/L_{G2} = 300 nm/100 nm. Dotted line in the left plot is for a standard HEMT, showing monotonic decrease with increase in gate bias. (after Ref. 9.)

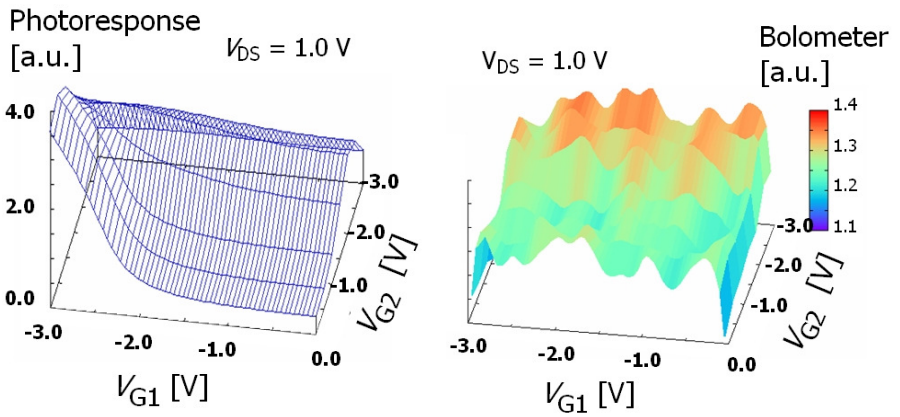

Fig. 11. (a) photoresponse and (b) 4K-cooled Si bolometer signal at V_{DS} =1.0 V for a metal grating-gate sample having a grating gates geometry of L_{G1}/L_{G2} = 300 nm/100 nm. (after Ref. 9)

maxima at $V_{G2} \approx$ -2.0 V along with the V_{G1} axis. In such a region, the bolometer shows clear enhancement of the signal. The observed signal is low and noisy due to atmospheric vapor absorption between the sample and the bolometer. According to well recognized responsivity on the order of 10^5 to 10^6 V/W for the Si composite bolometer used in this experiment (not calibrated) and atmospheric vapor absorption along with 20-cm propagation from the device to the bolometer, the emission power is roughly estimated to be 0.1 μW from a single device. When V_{G1} = -3 V and V_{G2} = 0 V, on the contrary, the photoresponse shows an increase but the bolometer doesn't detect the radiation. In this case, the photoresponse shows a non-resonant detection near to the threshold voltage. This phenomenon is well known as a space-charge effect of photoconductivity[30, 31]. Analytical calculation[3, 4, 9] indicates that the emission at a frequency around 1.3 to 1.8 THz should occur when $V_{G2} \approx$ -2.5 V and V_{G1} = 0 V for this sample, supporting the measured results.

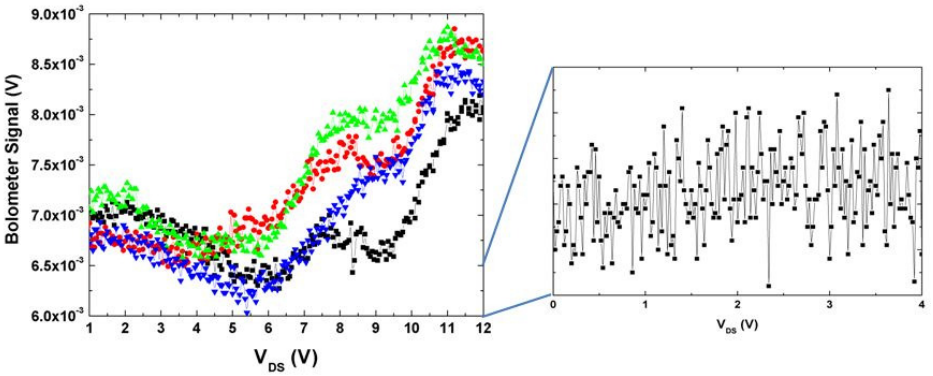

Fig. 12. Left: bolometer detection of emission from a semiconducting grating-gate sample with L_{G1}/L_{G2} = 150 nm/1850 nm at room temperature as a function of V_{DS}. Measurement took place four times. Right: the result from a metal grating-gate sample with L_{G1}/L_{G2} = 75 nm/350 nm for comparison. (after Ref. 23.)

The result of the bolometric measurement for a semiconducting grating-gate sample is shown in Fig. 12 as a function of V_{DS}[11, 23]. The V_{DS} increases to the knee voltage from which the transistor is operated in the saturation region. The bolometer signal starts increasing at around 6 V and two clear peaks are observed at 8 and 11 V. These features were observed with good reproducibility as shown in Fig. 12. Compared with the results for metal grating-gate sample, remarkable enhancement in emission intensity by one order of magnitude was obtained. Note that the V_{DS} range is larger than that for metal grating-gate samples because the double-decked HEMTs in this work suffer from large parasitic source and drain resistance. Nevertheless the double-decked device exhibits more drastic change in the bolometer signal with increasing V_{DS}. This result supports the idea of low-conductive gate stack to enhance the THz radiation efficiency[6, 22], and therefore indicates that the proposed double-decked HEMT structure is a promising candidate to realize solid-state THz-wave emitters with high power and large efficiency.

It is inferred, from such a phenomenological coincidence that the marked photoresponse of this work is attributed to the plasmon excitation due to the injection of photoelectrons accelerated by the strong electric field arisen at the plasmon cavity boundaries, leading to self-oscillation of emission of terahertz electromagnetic radiation. Significant improvement on the plasmon resonance is owing to the original dual-grating gate device structure.

2.4.3. *Two-photon injection-locked difference-frequency terahertz emission*

We conducted a so-called photomixing experiment. This is a trial for two-photon injection-locked difference-frequency terahertz generation. A pair of 1550-nm band tunable laser sources with an average power of 2 mW was used. The frequencies of those two laser sources are set so as to have a specific difference frequency Δf in the terahertz range. The polarizations of both beams are aligned be in parallel to the channel direction.

The illumination scheme is similar to that mentioned in 2.4.2. The emission spectra are measured using FTIR as described in 2.4.1.

The photogenerated electrons including terahertz Δf component are injected to the plasmon cavities. If Δf is close to the plasmon resonant frequency, the oscillation at Δf is promoted so that the neighboring frequency components may tend to be attracted to Δf. One can expect this gives rise to injection-locked coherent, monochromatic Δf generation.

The device used is a metallic grating gate type having a grating geometry of 70 nm and 1850 nm. First obtained preliminary results are shown in Fig. 13. Δf is set at 2.2 THz and 4 THz. For both cases, unfortunately, we could not yet succeed in injection-locking operation. However, when Δf is set at 2.2 THz which is close to 2.4 THz the background peak emission frequency, asymptotic behavior of injection locking to the Δf point is clearly observed. When Δf is detuned to 4 THz, the effect of frequency attraction is still observed but becomes weak.

The factors preventing from injection-locked oscillation are considered to be poor injection efficiency due to (i) broadband, intense background emission, and (ii) markedly long photoelectron life time (on the order of ns). Adding to the broadband hot plasmons emission dominating at higher V_{ds} as discussed in 2.4.1, dispersion of sheet carrier density along with the source-drain direction depending on applied V_{ds} is another factor that disperses the emission spectrum. Relatively low V_{ds} will help suppress this spectral broadening but the instability also weakens. Introduction of non-equal finger-size grating compensating for the electron density dispersion would be a solution. As mentioned in 2.4.2, the GaAs-based material systems used in the present device is transparent to the 1550-nm photons so that two-photon process via deep trap centers at the InGaAs/GaAs heterointerface takes place. Those photoelectrons have considerably long carrier life time which significantly attenuates the terahertz Δf photoelectron components. Introduction of InP material systems would be a solution.

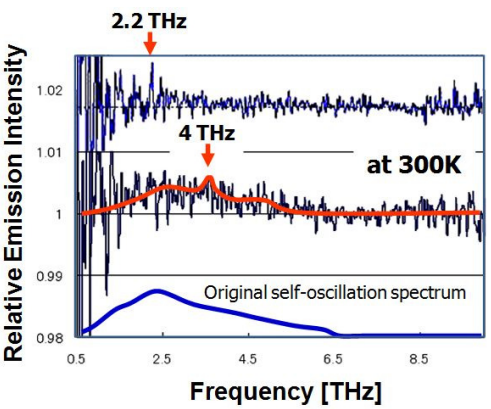

Fig. 13. Emission spectra when the device is subject to two-photon laser illumination at 300K, exhibiting asymptotic behavior of injection locking to the difference frequency (Δf) point. Δf is set at 2.2 THz (upper) and 4 THz (middle). The lower curve is an original self-oscillation spectrum without optical excitation (not scaled vertically).

2.4.4. *Impulsive laser excited terahertz emission*

Electromagnetic response to impulsive photoexcitation was also measured at room temperature by using reflective electrooptic sampling[7, 9]. A 1550-nm, 1-mW, 70-fs laser pulse was used as pump and probe beams. When the sample was appropriately biased, as shown in Fig. 14(a), it emitted an impulsive radiation followed by monochromatic relaxation oscillation which was significantly enhanced by its vertical cavity structure. The Fourier spectrum exhibited resonant peaks at 0.8 THz and its harmonic frequencies of up to 3.2 THz as shown in Fig. 14(b). These results are attributed to the emission of coherent electromagnetic radiation stimulated by photo-induced plasmon instability. Estimated radiation power would exceed 0.1 μW. We confirmed that the emission spectrum traces the 2D plasmonic dispersion relation in terms of its 2D electron density and the cavity size[8, 9].

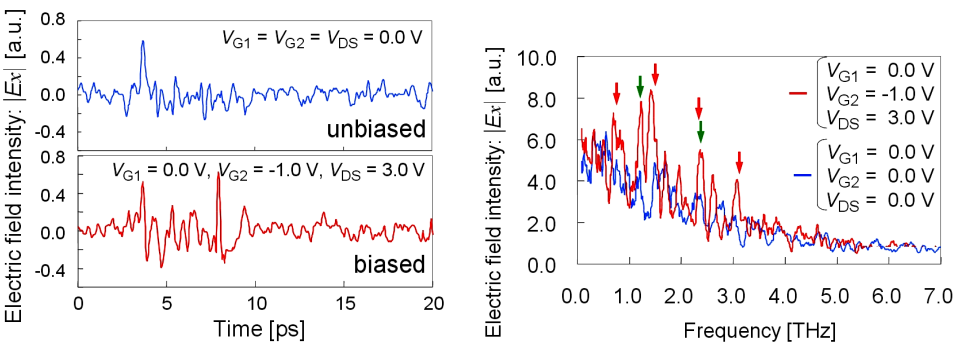

Fig. 14. Field emission response to impulsive photoexcitation. Grating gates geometry: L_{G1}/L_{G2} = 350 nm/70 nm. Left: temporal response, right: Fourier spectra. (after Ref. 9.)

3. Terahertz Intensity Modulator Based on Controlling 2D Plasmon Dispersion

One can consider the device structure as a gated functional element as shown in Fig. 15[32-35]. Suppose that the data signal is input to one gate grating so as to modulate the sheet electron density of the plasmonic cavity grating, and that a terahertz carrier wave is input to the device. If the intensity of the transmitted wave is sufficiently modulated by the gate bias, the data can be coded onto the terahertz carrier wave. Due to the high-speed nature of the HEMT structure, it is easy to perform the data coding at tens of Gbit/s onto the terahertz carrier[33]. Based on the above mentioned 2D-plasmonic nanostructure, we numerically analyze the dispersive effect on the transmission spectrum for coherent terahertz electromagnetic (EM) waves, and demonstrate functionalities of terahertz frequency multipliers as well as intensity modulators.

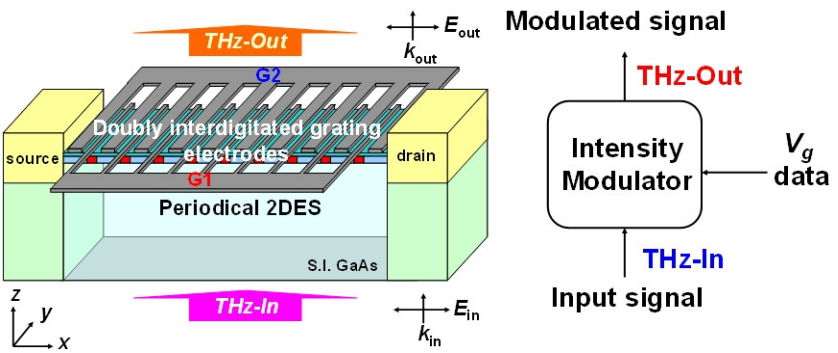

Fig. 15. Double-grating plasmonic nanostructure configuring intensity modulator.

Physical phenomena of 2D plasmons are described by the hydrodynamic equations. According to the Mikhailov's theory[13], after liberalized approximation the permittivity and conductivity of 2D plasmons are led to the following form[13, 33]:

$$\varepsilon(k,\omega) = \varepsilon_\infty + \frac{\pi d k^2 n e^2}{\varepsilon_0 m} \frac{i}{(\omega - k v_d)(\omega - k v_d + i\tau^{-1})}$$
$$\sigma(k,\omega) = \frac{n e^2}{m} \frac{i\omega}{(\omega - k v_d)(\omega - k v_d + i\tau^{-1})} \tag{3}$$

where ε_∞ the permittivity at finite frequency, ε_0 the permittivity in vacuum, d the gate-channel distance, n the density of electrons, e the electronic charge, m the effective mass, v_d the drift velocity, τ the total momentum relaxation time, ω the angular frequency, k the wave vector of the grating geometry. This Mikhailov's dispersive plasmonic conductivity is similar to the Drude-optical conductivity including n and ω, but is different and featured by two distinctive parameters having k and v_d. Based on Eq. (3), we can electronically control the dispersion by changing n and v_d due to the relation of the gate and drain bias voltages. We will implement the conductivity Eq. (3) into our in-house Maxwell's FDTD (Finite-Differential Time-Domain) simulator.

Figure 16 shows typical spatial field distributions of the electric field intensity (E_x) on the device cross section at a specific time step[32, 33]. The electron drift velocity v_d is fixed at 2×10^7 cm/s. When n is set at a relatively low value (2.2×10^9 cm^{-2}), the electric field intensity distributes monotonically so that a *radiative* mode of transverse-electric (TE) waves is excited. This is because, in this case, the fundamental mode of plasmons is dominantly excited to be coupled with the *zero* mode of TE waves. On the other hand, when n is set at a relatively high value (1.6×10^{12} cm^{-2}), anti-parallel electric field is excited with respect to the center of the channel. The electric filed intensity is cancelled out and *non-radiative* mode of TE waves is developed. This is because, in this case, the second harmonic mode of plasmons is predominantly excited to be coupled with the *first* mode of the TE waves. These results imply that the *radiative* or *non-radiative* mode is

directly reflected by the density of electrons in the plasmon cavities. The mode coupling property is also affected by v_d. With increasing v_d, the threshold value of n at which the mode coupling shifts from *radiative* to *non-radiative* goes high. Detail discussion will be given in Ref. 35.

Figure 17 summarizes the field emission spectra for various n_{sp} conditions. In the frequency range from 0 to 4 THz, the field intensity decreases with increasing n_{sp} [33]. We speculate that transmission property for terahertz electromagnetic waves is markedly modulated by controlling n_{sp}, thus, the gate bias voltage. We further investigate the frequency dependence of the modulation efficiency or extinction ratio of the device. Figure 18 shows the typical results[34]. The field intensity is modulated by n_{sp}. With

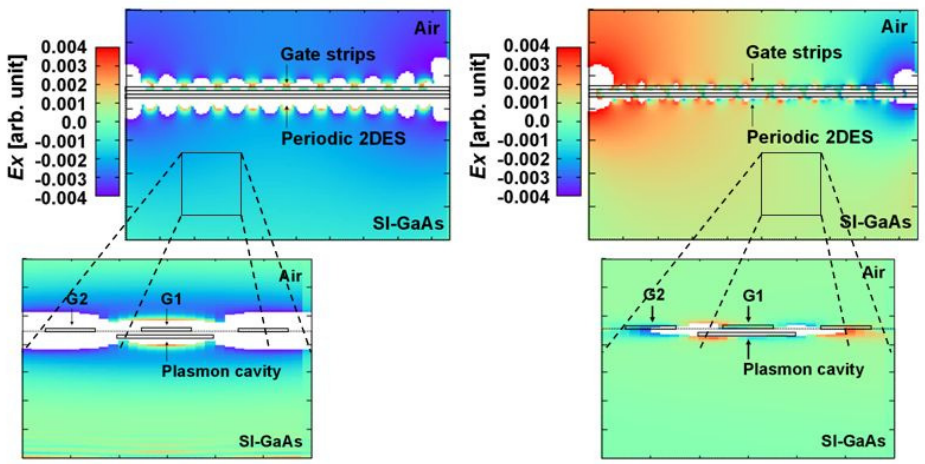

Fig. 16. Simulated spatial distribution of electric field intensity E_x at n_{sp} = 2.2 x 10^9 cm^{-2} (left) and n_{sp} = 1.6 x 10^{12} cm^{-2} (right). v_d = 2 x 10^7 cm/s. (after Ref. 33.)

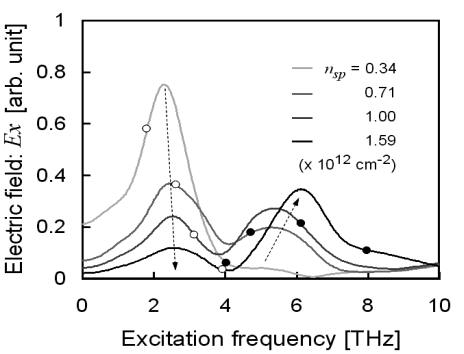

Fig.17. Field emission spectra for various n_{sp} conditions ○: fundamental plasmon mode, ●: 2nd harmonic plasmon mode. (after Ref. 32.)

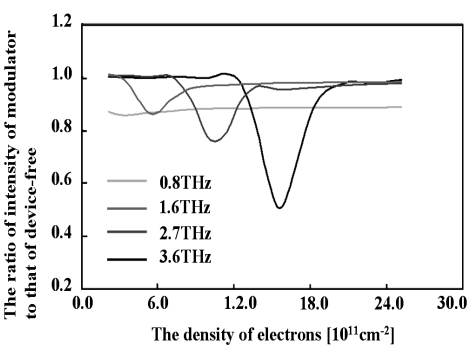

Fig. 18. Normalized intensity of transmitted electromagnetic waves vs. n_{sp} for various terahertz carrier frequencies. (after Ref. 34.)

increasing the frequency of the EM wave, its intensity modulation can be performed in higher n_{sp} region with higher modulation efficiency. The extinction ratio defined as the ratio of the maximum to the minimum intensity is 3% at 0.8 THz, 15% at 1.6 THz, 24% at 2.7THz and 49% at 3.6THz, respectively. Note that the result for 0.8 THz showing a flat-band response with less intensity is due to the surface plasmon resonance at the grating gates.

Figure 17 also suggests another important aspect. For each spectrum, according to n_{sp}, the fundamental and 2nd harmonic plasmon resonances stay around 2~4 THz and 4~8 THz, respectively. Thus, it is seen that with increasing n_{sp}, the fundamental mode is suppressed while the 2nd mode becomes dominant. Therefore, the device can act as a terahertz frequency multiplier[32]. The above results demonstrate the electrically controllable dispersive effects on the transmission spectrum of a plasmon-resonant grating-gate HEMT device giving rise to potential functionality of a terahertz signal processing.

4. Conclusion

Recent advances in novel plasmonic nanotransistors for emission and intensity modulation of terahertz electromagnetic waves were reviewed. Material- and structure-dependent highly dispersive systems were configured with submicron-to-nanometer scaled 2D grating structures in a HEMT device. Analytical and Experimental studies revealed its various potential functionalities including emission, detection, intensity modulation, as well as frequency multiplication in the exploring terahertz frequency regime.

Acknowledgements

The authors would like to acknowledge Prof. T. Asano at Kyuhsu University, Japan, and all the students in Otsuji and Sano Laboratories for their extensive contributions throughout this work. They also thank Prof. W. Knap at Tohoku University, Japan (on leave from CNRS, France), Drs. D. Coquillat and F. Teppe at GES-UMR5650, CNRS and Montpellier 2 University, France for their experimental support and Prof. Victor Ryzhii at Univ. of Aizu, Japan and Prof. V.V. Popov and Dr. G.M. Tsymbalov at Inst. Radio Eng. Electron., Saratov Branch, Russia for their theoretical support, and Prof. K. Narahara at Yamagata University, Japan, Prof. M. Dyakonov at Montpellier 2 University, France, and Prof. M. Shur at Rensselaer Polytechnic Institute for many helpful discussions. This work was financially supported in part by the SCOPE Programme from the MIC, Japan, and by the Grant in Aid for Basic Research (S) from the JSPS, Japan.

References

1. M. Tonouchi, “Cutting-edge terahertz technology,” Nature Photon., **1**, 97-105(2007).
2. H.-T. Chen, W.J. Padilla1, J. M.O. Zide, A.C. Gossard, A.J. Taylor and R.D. Averitt, “Active terahertz metamaterial devices,” Nature, **444**, 597-600(2006).

3. M. Dyakonov, and M. Shur, “Shallow water analogy for a ballistic field effect transistor: new mechanism of plasma wave generation by dc current,” Phys Rev Lett **71**, 2465-2468 (1993).
4. M. Dyakonov, and M. Shur, “Detection, mixing, and frequency multiplication of terahertz radiation by two dimensional electronic fluid,” IEEE Trans. Electron Devices **43**, 380-387 (1996).
5. J. Lusakowski, “Nanometer transistors for emission and detection of THz radiation,” Thin Solid Films **515**, 4327-4332 (2007).
6. T. Otsuji, M. Hanabe, T. Nishimura, and E. Sano, “A grating-bicoupled plasma-wave photomixer with resonant-cavity enhanced structure,” Opt. Express **14**, 4815-4825 (2006).
7. T. Otsuji, Y. M. Meziani, M. Hanabe, T. Ishibashi, T. Uno, and E. Sano, “Grating-bicoupled plasmon-resonant terahertz emitter fabricated with GaAs-based heterostructure material systems,” Appl. Phys. Lett. **89,** 263502 (2006).
8. Y. M. Meziani, T. Otsuji, M. Hanabe, T. Ishibashi, T. Uno, and E. Sano, “Room temperature generation of terahertz radiation from a grating-bicoupled plasmon-resonant emitter: Size effect ,” Appl. Phys. Lett. **90**, 061105 (2007).
9. T. Otsuji, Y.M. Meziani, M. Hanabe, T. Nishimura, and E. Sano, “Emission of terahertz radiation from InGaP/InGaAs/GaAs grating-bicoupled plasmon-resonant emitter,” Solid-State Electron. **51**, 1319-1327 (2007).
10. Y. M. Meziani, H. Handa, W. Knap, T. Otsuji, E. Sano, V. V. Popov, G. M. Tsymbalov, D. Coquillat, and F. Teppe, "Room temperature terahertz emission from grating coupled two-dimensional plasmons," Appl. Phys. Lett. **92**, 201108 (2008).
11. T. Otsuji, Y. M. Meziani, T. Nishimura, T. Suemitsu, W. Knap, E. Sano, T. Asano, V.V. Popov, “Emission of terahertz radiation from dual-grating-gates plasmon-resonant emitters fabricated with InGaP/InGaAs/GaAs material systems,” J. Phys. Cond. Matt. **20**, 384206 (2008).
12. R.J. Wilkinson, C.D. Ager, T. Duffield, H.P. Hughes, D.G. Hasko, H. Armed, J.E.F. Frost, D.C. Peacock, D.A. Ritchie, A.C. Jones, C.R. Whitehouse, and N. Apsley, “Plasmon excitation and self-coupling in a bi-periodically modulated two-dimensional electron gas,” J. Appl. Phys., **71**, 6049-6061(1992).
13. S.A. Mikhailov, “Plasma instability and amplification of electromagnetic waves in low-dimensional electron systems ,” Phys. Rev. B, 58, 1517-1532 (1998).
14. V. Ryzhii, A. Satou, and M. Shur, “Plasma instability and amplification of electromagnetic waves in low-dimensional electron systems ,” IEICE Trans. Electron. **E89-C**, 1012-1019 (2006).
15. V. Ryzhii, A. Satou, M. Ryzhii, T. Otsuji, and M. S. Shur, "Mechanism of self-excitation of terahertz plasma oscillations in periodically double-gated electron channels," J. Phys. Cond. Matt. **20**, 384207 (2008).
16. R. A. Hopfel, E. Vass, and E. Gornik, “Thermal excitation of two-dimensional plasma oscillations,” Phys. Rev. Lett. **49**, 1667 (1982).
17. D. C. Tsui, E. Gornik and R. A. Logan, “Far infrared emission from plasma oscillations of Si inversion layers ,” Solid State Comm. **35**, 875-877 (1980).
18. N. Okisu, Y. Sambe, and T. Kobayashi, “Far-infrared emission from two-dimensional plasmons in AlGaAs/GaAs heterointerfaces,” Appl. Phys. Lett. **48**, 776-778 (1986).
19. R. Hopfel, G. Lindemann, E. Gornik, G. Stangl, A. C. Gossard and W. Wiegmann, “Cyclotron and plasmon emission from two-dimensional electrons in GaAs,” Surf. Sci. **113**, 118-123 (1982).

20. K. Hirakawa, K. Yamanaka, M. Grayson and D. C. Tsui, "Far-infrared emission spectroscopy of hot two-dimensional plasmons in Al0.3Ga0.7As/GaAs heterojunctions," Appl. Phys. Lett. **67**, 2326-2328 (1995).
21. M. Hanabe, N. Imamura, T. Uno, T. Ishibashi, Y. M. Meziani and T. Otsuji, "Effects of parasitic capacitance on the terahertz plasmon resonance in GaAs MESFET's," in Extended Abstracts of the International Workshop on Terahertz Technology 2005, 181-182 (2005).
22. M. Hanabe, T. Nishimura, M. Miyamoto, T. Otsuji and E. Sano, "Structure-sensitive design for wider tunable operation of terahertz plasmon-resonant photomixer," IEICE Trans. Electron. **E89-C**, 985-992 (2006).
23. T. Suemitsu, Y.M. Meziani, Y. Hosono, M. Hanabe, T. Otsuji, E. Sano, "Novel plasmon-resonant terahertz-wave emitter using a double-decked HEMT structure" 65th Device Research Conference (DRC) Dig., 157-158 (2007).
24. T. Nishimura, H. Handa, H. Tsuda, T. Suemitsu, Y.M. Meziani, W. Knap, T. Otsuji, E. Sano, V. Ryzhii, A. Satou, V.V. Popov, D. Coquillat, and F. Teppe, "Broadband Terahertz Emission from Dual-Grating Gate HEMT's -Mechanism and Emission Spectral Profile," 66th Device Research Conference (DRC) Dig. 236-237 (2008).
25. J. A. Porto, F. J. Garchia-Vidal, and J. B. Pendry, "Transmission resonances on metallic gratings with very narrow slits," Phys. Rev. Lett. **83**, 2845-2848 (1999).
26. V. V. Popov, O. V. Polischuk, T. V. Teperik, X. G. Peralta, S. J. Allen, N. J. M. Horing, and M. C. Wanke, "Absorption of terahertz radiation by plasmon modes in a grid-gated double-quantum-well field-effect transistor," J. Appl. Phys. **94**, 3556-3562 (2003).
27. V. V. Popov, G. M. Tsymbalov, and N. J. M. Horing, "Anticrossing of plasmon resonances and giant enhancement of interlayer terahertz electric field in an asymmetric bilayer of two-dimensional electron strips," J. Appl. Phys. **99**, 124303 (2006).
28. T. Otsuji, M. Hanabe and O. Ogawara, "Terahertz plasma wave resonance of two-dimensional electrons in InGaP/InGaAs/GaAs high-electron-mobility transistors," Appl. Phys. Lett. **85**, 2119 (2004).
29. E. Sano, "Simulation of carrier transport across heterojunctions based on drift–diffusion model incorporating an effective potential," Jpn. J. Appl. Phys. **41**, L1306–L1308 (2002).
30. Y. Takanashi, K. Takahata, Y. Muramoto, "Characteristics of InAlAs/InGaAs high-electron-mobility transistors under illumination with modulated light," IEEE Trans. Electron Dev. **46**, 2271-2277 (1999).
31. M.S. Shur, J.-Q. Lu, "Terahertz sources and detectors using two dimensional electronic fluid in high electron-mobility transistors," IEEE Trans. Microwave Theory Tech. **48**, 750-756 (2000).
32. T. Nishimura, M. Hanabe, M. Miyamoto, T. Otsuji, and E. Sano, "Terahertz plasma wave resonance of two-dimensional electrons in InGaP/InGaAs/GaAs high-electron-mobility transistors," IEICE Trans. Electron. **E89-C**, 1005-1011 (2006).
33. T. Nishimura and T. Otsuji, "Terahertz polarization controller based on electronic dispersion control of 2D plasmons," International Journal of High Speed Electronics and Systems **13**, 547-555 (2007).
34. T. Nishimura, K. Horiike, and T. Otsuji, "A novel intensity modulator for terahertz electromagnetic waves utilizing plasmon resonance in grating-gate HEMT's," 7th Topical Workshop on Heterostructure Microelectron., 67-68 (2007).
35. T. Nishimura, N. Magome, and T. Otsuji, "A novel intensity modulator for terahertz electromagnetic waves utilizing two-dimensional plasmon resonance in a dual-grating-gate high electron mobility transistor," submitted to Jpn. J. Appl. Phys.